Journal of Experimental Botany Advance Access published June 26, 2007

Journal of Experimental Botany, Page 1 of 11
doi:10.1093/jxb/erm116
This paper is available online free of all access charges (see http://jxb.oxfordjournals.org/open_access.html for further details)

Journal of Experimental Botany
www.jxb.oxfordjournals.org

RESEARCH PAPER

Non-destructive diffraction enhanced imaging of seeds

Lester W. Young[1,*], Christopher Parham[2], Zhong Zhong[2], Dean Chapman[3] and Martin J. T. Reaney[4,†]

[1] *Agriculture and Agri-Food Canada, 107 Science Place, Saskatoon, SK, Canada S7N 0X2*

[2] *National Synchrotron Light Source, Brookhaven National Laboratory, Upton, NY 11973, USA*

[3] *Department of Anatomy and Cell Biology, 107 Wiggins Road, University of Saskatchewan, Saskatoon, SK, Canada S7N 5E5*

[4] *Department of Applied Microbiology and Food Science, 51 Campus Drive, University of Saskatchewan, Saskatoon, SK, Canada S7N 5A8*

Received 1 February 2007; Revised 26 April 2007; Accepted 30 April 2007

Abstract

Techniques that make possible the non-destructive continuous observation of plant anatomy and developmental processes provide novel insights into these phenomena. Non-destructive imaging of seeds was demonstrated using the synchrotron-based X-ray imaging technique, diffraction enhanced imaging (DEI). The seed images obtained had good contrast and definition, allowing anatomical structures and physiological events to be observed. Structures such as hypocotyl–root axes, cotyledons, seed coats, air cavities, and embryo-less *Brassica napus* L. seeds were readily observed using DEI. Embryo axes, scutella, pericarp furrows, coleoptiles, and roots were observable over a time-course in individual germinating *Triticum aestivum* L. caryopses. Novel anatomical and physiological observations were also made that would have been difficult to make continuously using other techniques. The physical principles behind DEI make it a unique imaging technique. Contrast in DEI is the result of X-ray refraction at the density differences occurring at tissue boundaries, scatter caused by regions containing ordered molecules such as cellulose fibres, and attenuation. Sectioning of samples and the infusion of stains or other contrast agents are not necessary. Furthermore, as high-energy X-rays are used (30–40 keV), little X-ray absorption occurs, resulting in low levels of radiation damage. Consequently, studies of developmental processes may be performed on individuals. Individual germinating *B. napus* and *T. aestivum* seeds were imaged at several time points without incurring any apparent radiation damage. DEI offers a unique way of examining plant anatomy, development, and physiology, and provides images that are complementary to those obtained through other techniques.

Key words: Diffraction enhanced imaging, NMR imaging, seed anatomy, tissue density, X-ray attenuation and refraction, X-ray imaging.

Introduction

Non-destructive imaging techniques are powerful tools that allow us rapidly to improve our knowledge of plant function and development. Some examples include radiography (Milner *et al*., 1952*a*; Pechen and Keller, 1988), nuclear magnetic resonance (NMR) (Jenner *et al*., 1988; Manz *et al*., 2005), confocal microscopy (Haseloff, 2003), X-ray phase contrast imaging (PCI) or tomography (Paris *et al*., 2000; Hwu *et al*., 2004; Cloetens *et al*., 2006), and optical projection tomography (OPT) (Lee *et al*., 2006). In this paper, the ability of a synchrotron-based imaging technique, diffraction enhanced imaging (DEI) (Chapman *et al*., 1997), to image soft plant tissues, namely seeds, is demonstrated. It is suggested that DEI will be useful for imaging plant structures, development, and some aspects of physiology, and that it is complementary to other imaging techniques.

Most work describing DEI to date has focused on demonstrating the use of this X-ray-based technique for

* Present address: Department of Plant Science, 51 Campus Drive, University of Saskatchewan, Saskatoon, SK, Canada S7N 5A8.
† To whom correspondence should be addressed. E-mail: martin.reaney@usask.ca

Abbreviations: DEI, diffraction enhanced imaging; MIR, multiple image radiography; PCA, principle component analysis; PCI, phase contrast imaging; OPT, optical projection tomography.

medical imaging (Mollenhauer *et al*., 2002; Li *et al*., 2003; Wernick *et al*., 2003; Muehleman *et al*., 2006). Examination of animal tissues with DEI allowed different soft tissue types, such as skin, muscle, and tendon, to be observed in detail which is not possible using conventional radiography. Based on the principles underlying DEI, it was hypothesized that this technique could provide novel images of plant soft tissues. The novel data provided by continuous or repeated observations of the same organism would be difficult or impossible to obtain by other means.

The three principle ways X-rays interact with matter are absorption, refraction, and scatter. Table 1 summarizes the relevant interactions between X-rays and matter. Conventional radiography uses X-ray absorption to derive contrast; however, samples also refract and scatter photons. The refracted and scattered photons cause noise in the image and reduce edge definition. By comparison, DEI separates refracted X-ray photons from non-refracted ones and measures them separately (Chapman *et al*., 1997; Li *et al*., 2003; Wernick *et al*., 2003; Muehleman *et al*., 2006). Typically a DEI data set consists of two or more images, an attenuation image (photons hitting the detector without being refracted, scattered, or absorbed) and one or more refraction images. Together, the refraction and attenuation images produce low-noise images with sharp definition. This is because only photons that are not absorbed, refracted, or scattered are observed in the attenuation image and only photons refracted at a particular angle are observed in any single refraction image.

As mentioned above, DEI quantifies refraction, scatter, and, by deduction, attenuation separately. Density differences in a sample result in X-ray refraction, while atoms or molecules ordered parallel to the beam cause scatter. In other words, DEI allows observations of the boundaries between tissues that have different densities (Mollenhauer *et al*., 2002; Li *et al*., 2003), as well as regions with high concentrations of regularly arranged molecules such as starch, cellulose fibres, or protein storage bodies (Bouwstra *et al*., 1993; Jenkins *et al*., 1993; Donald *et al*., 2001). The degree of refraction and scatter occurring is related to the density difference at the tissue boundaries and the overall concentration of scattering molecules.

Separation of the attenuation, refraction, and scatter data is achieved in DEI by placing an 'analyser crystal' (flat silicon crystal) between the sample and the detector. The analyser crystal acts like a mirror, but only reflects those photons impinging on it at a particular angle (the Bragg angle for the crystal and energy/wavelength of X-rays used) to the detector. Photons hitting the analyser at angles other than the Bragg angle are not sent onto the detector, i.e. only those photons propagating from the sample at a precise angle are detected. Photons refracted by the sample at a different angle may be detected by rotating the analyser crystal and detector relative to the sample. The Bragg angle for the analyser crystal remains the same; however, only photons propagating from the sample at the new angle of incidence are reflected onto the detector. Collecting images at different analyser crystal angles allows an intensity versus angle curve, the 'rocking curve', to be calculated. A modified version of DEI, called multiple image radiography (MIR) (Wernick *et al*., 2003; Muehleman *et al*., 2006), records the rocking curve for each pixel and uses these data to calculate the attenuation, refraction, and ultra-low angle scattering images. The quality of both DEI and MIR images is high. Excellent clarity of complex, overlying features is often obtained using MIR.

Conventional radiography uses relatively low-energy X-rays in order to obtain sufficient contrast as soft tissues poorly absorb higher energy photons. Previous work used X-rays in the 12–15 keV range to image seeds (Foucat *et al*., 1993; de Carvalho *et al*., 1999; Haff and Slaughter, 2004). Unfortunately, lower energy X-rays cause greater levels of radiation damage as greater amounts of energy are absorbed by the sample. As refraction and scatter provide information for DEI rather than absorption, higher energy X-rays are used, typically in the 30–40 keV range, greatly reducing absorbed radiation doses. The lower X-ray doses absorbed by samples during DEI make this technique useful for studying development as radiation damage artefacts are avoided.

Table 1. *X-ray interactions with matter*

Abbreviations: DEI, diffraction enhanced imaging; MIR, multiple imaging radiography.

Interaction	Attenuation	Refraction	Scatter
Measured using:	Conventional X-ray imaging, DEI, MIR	DEI, MIR	MIR
Observed as:	Loss of X-rays reaching detector	Bending of X-ray propagation path	Broadening of beam
Due to:	Absorption, refraction or scattering of X-rays	Changes to speed of X-rays propagating through matter of differing densities	Changes in distribution of beam occurring at sub-pixel level
Enables observation of:	Dense tissues (e.g. wood, highly refractive or scattering tissues, by subtraction)	Density differences such as tissue boundaries (e.g. boundary between cotyledons and hypocotyl-root axis)	Structures containing order at the cellular or molecular level (e.g. cells parallel to the incident beam or cellulose, starch, oleosomes)

Some of the advantages that make DEI a useful tool for examining plant structures include the ability to observe objects *in situ*, its non-destructiveness, and ease of sample preparation. Techniques such as confocal microscopy, NMR imaging, and conventional radiography share these advantages; however, the data obtained by each of these techniques uses a different physical principle. These similarities and differences make these techniques highly complementary. Unique to DEI is imaging based on density and areas containing atomic order.

Here the use of DEI to examine seed anatomy and to identify entrained air cavities is described. Also the use of DEI to examine *Brassica napus* L. (canola) seed anatomy and to observe both canola and *Triticum aestivum* L. (wheat) germination over a time course is demonstrated.

Materials and methods

Sample preparation

Brassica napus L. (canola) and *Triticum aestivum* L. (wheat) were grown on the AAFC farm, Saskatoon.

Initial images were made of canola seeds embedded in discs of Epon Araldite (Structure Probe Inc., West Chester, PA, USA). The number of air bubbles in the embedding material was minimized by hardening the discs in their moulds overnight under vacuum (26 mmHg) at 80 °C. For imaging, the discs were submerged in water.

Previous work showed a relationship between fatty acid content, density, and seed maturity in canola seeds (Young *et al*., 2006). The object of the present study was to determine if seeds with different densities (due to both fat content and air cavities) could be distinguished using NMR and DEI. Canola seeds were sorted into $d < 1.00$, $d < 1.04$, $d < 1.08$, $d < 1.13$, and $d > 1.13$ density groups using low-polarity food-grade media as described previously (Young *et al*., 2006). Each of the groups, except the $d > 1.13$ fraction, was further separated into groups with air cavities (+), which sank in the density medium when placed under pressure, and those without air cavities (–), which floated. After sorting, the seeds were washed several times with 95% ethanol and allowed to air dry. Cyanoacrylate (Loctite Brand, Henkel Consumer Adhesives) was used to stick seeds from each pressure density-sorted fraction to optically clear Lucite discs. The discs were photographed and then imaged using NMR and DEI.

To observe germination, canola seeds and wheat caryopses were glued to pipette tips using cyanoacrylate. The pipette tips were attached to the lid of a Magenta jar (Magenta Corporation, Chicago, IL, USA). The Magenta jars were half filled with water and inverted for imbibition and imaging. During periods when the seeds were not being imaged, the jars were stored upright (to prevent water logging of the seeds), at room temperature, and in the dark, except during the initial 4 h when they were kept inverted. For canola, DEI data were recorded 0, 2, 4, 8, 20, 44, 56, 116, and 146 h after imbibition; with wheat an additional image was developed at 156 h.

Diffraction enhanced imaging

Seeds were imaged using DEI at the National Synchrotron Light Source-Brookhaven National Laboratory (NSLS-BNL), beamline X15A. The discs were submerged in ethanol or distilled water and imaged with a 40 keV beam. A silicon (333) analyser crystal was placed after the sample stage and rotated using 1 μrad steps to capture only those photons striking it at the correct Bragg angle. Separated by 1 μrad steps, 11, 21, or 31 images were captured in addition to a background image which was made with the beam shutter closed. Photons reflected from the analyser crystal were captured using a Fuji HR-V image plate with a Fuji BAS-2500 reader, taking approximately 30 s to record each image. Pixel size was 50 μm×50 μm.

DEI data processing

Beamline control and data collection were handled by a program called spec (Certified Scientific Software, Cambridge, MA, USA). The data were subsequently manipulated and images displayed using Igor Pro 5.04 (Wavemetrics, Lake Oswego, OR, USA). Each vertical column of image data was normalized, using a region of the image that did not contain any sample, to reduce differences in detector sensitivity. The average intensity and standard deviation of each pixel's rocking curve was determined and used in a grey-scale image as a means of reducing the dimensionality of the data.

The data were ordered into a three-dimensional array, with the x and y dimensions corresponding to the spatial coordinates of the image and the z dimension corresponding to the rocking curve angle, i.e. each of the 11, 21, or 31 points in the z dimension represented a different angle on the rocking curve. Correlation principle component analysis (PCA) of the three-dimensional array was performed using HyperCube (US Army Topographic Engineering Centre, http://www.tec.army.mil/Hypercube). Eigenvalues for the first two or three PCA images (out of 11, 21, or 31 component images) were typically greater than 2.2. Variation in the rocking curve for each pixel in the image is extracted with each component of the PCA. HyperCube was also used to assign the first three components of the PCA to the red, green, or blue channels of the false colour images in the Supplementary data at *JXB* online.

NMR imaging

NMR imaging of the density-sorted seeds adhered to the Lucite discs was performed at the National Research Council/Plant Biotechnology Institute using five scans on an Avance WB machine operating at 360 Mhz (Bruker). 'Slices' 5 mm thick through the plane of the disc were used so that the NMR image of the whole seed was captured. Pixel size was approximately 21 μm×21 μm. See Pietrzak *et al*. (2002) for further details.

Results

Canola seeds could be distinguished from the Epon Araldite they were embedded in using DEI (Fig. 1) as they refract X-rays to a greater extent than the surrounding matrix. Darker pixels in the attenuation image (Fig. 1A) indicate regions where greater refraction or scatter occurred. Anatomical features such as hypocotyl–root axes, cotyledons, and seed coats could be observed (see Supplementary Fig. S1, available at *JXB* online, for a schematic of canola seed anatomy). The hypocotyl–root axis in cross-section strongly refracted X-rays, possibly due to alignment of the ground meristem cells, which are arranged in files parallel to the incident beam. The outline of hypocotyls in longitudinal section could also be observed (Fig. 1C); however, the intensity of refracted X-rays in the middle of these organs was not as great as when observed in cross-section, i.e. hypocotyl–root axes in longitudinal section were defined by X-ray refraction occurring at the tissue boundary with the cotyledons.

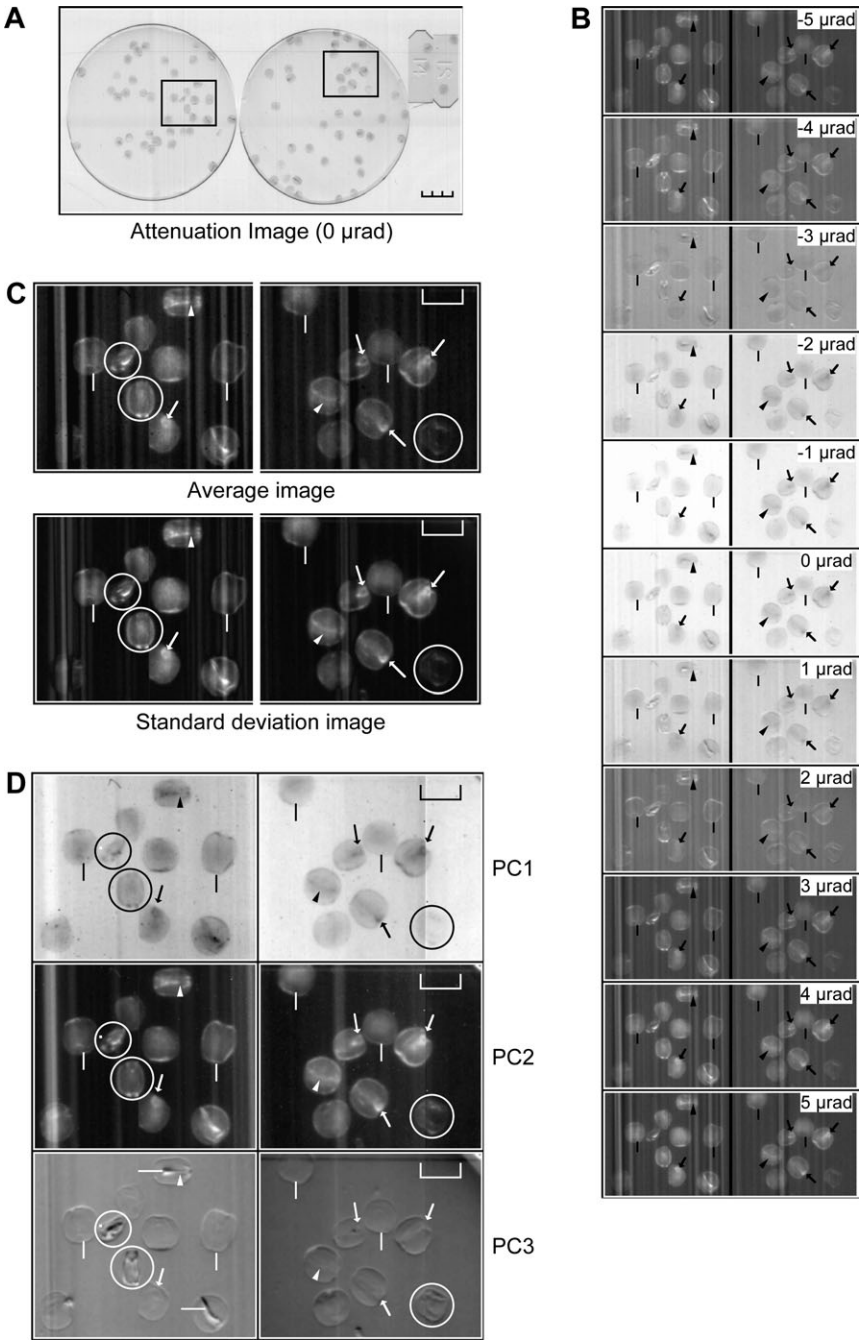

Fig. 1. Diffraction enhanced imaging of canola seeds embedded in Epon. (A) Attenuation image of soft tissues (seeds) imaged using DEI. Dark pixels indicate where X-rays have been attenuated through refraction or scattered. Graduations on the scale bar = 2 mm. (B) Magnified portions of (A) showing all 11 images in the DEI data set: hypocotyl–root axes in cross-section (arrows), longitudinal section (arrow heads), and seed coats (lines). Hypocotyls in cross-section and seed coats refract X-rays at approximately 5 µrad and 3 µrad, respectively. (C) Average and standard deviation images of the regions shown in (B). Misshapen seeds are more visible (circled). Scale bar = 2 mm. (D) The first two components from the PCA give clearer images similar to the attenuation (PC1) and refraction (PC2) images. The third component shows details of the cotyledons as well as air cavities (horizontal lines) trapped next to the hypocotyl–root axis of some seeds and within the misshapen seeds. Scale bar = 2 mm.

Hypocotyls in cross-section refracted X-rays by at least 5 µrad while maximal refraction for the seed coats occurred at ±3 µrad (Fig. 1B).

Non-anatomical features, such as air cavities appressed to the hypocotyl–root axis and misshapen seeds (Fig. 1C, D), were observed after analysis of the rocking curves was performed, i.e. average, standard deviation calculated for each pixel, and PCA performed. These features strongly refracted or scattered X-rays and were most observable in the third component of the PCA. The first two components of the PCA appeared similar to the attenuation and refraction images, but without as much noise. In the third

component image, the greatest contrast was derived from air cavities, seed coats, and misshapen seeds. This suggests that, with these data, the third component shows maximal density differences, such as occur where air pockets or seed coats are adjacent to surrounding tissues. In some seeds, the outline of the inner cotyledon could also be identified. Details were defined better visually when each component was assigned a colour in a red–green–blue image (see Supplementary Fig. S2 available at *JXB* online).

Photographs, NMR, and DEI images of canola seeds sorted according to density were compared (Fig. 2 and Supplementary Fig. S3 available at *JXB* online). In the photographs the hypocotyl–root axis and cracks in the seed coat could be observed. A 5 mm slice encompassing all the seeds was used in the NMR to increase the similarity to DEI, which records transmission data. The oil-rich cotyledons were visible in the NMR images, with the lower-intensity hypocotyl–root axes visible mainly through contrast against the cotyledons. Seeds in the lower-density fractions were expected to have a higher oil content and were typically brighter in the NMR images. The observations of canola seeds with the hypocotyl–root axis in cross-section look very similar to thin slices from NMR images of canola seeds in the same orientation (data not shown), with the procambium, ground meristem, and division between the cotyledons observable. One difference between the DEI and NMR images is that seed coats were observed in the former but not the latter.

PCA analysis was performed on the DEI data set from the density-sorted canola seeds. Anatomical features that were observed in the first two component images included seed coat, hypocotyl–root axis, and, in some cases, cotyledon outlines. Air cavities associated with the hypocotyl–root axis were also observed (Fig. 2, arrows).

Changes to the anatomy of germinating canola and wheat were observed using DEI (Figs 3 and 4 and Supplementary Figs S4 and S5 available at *JXB* online).

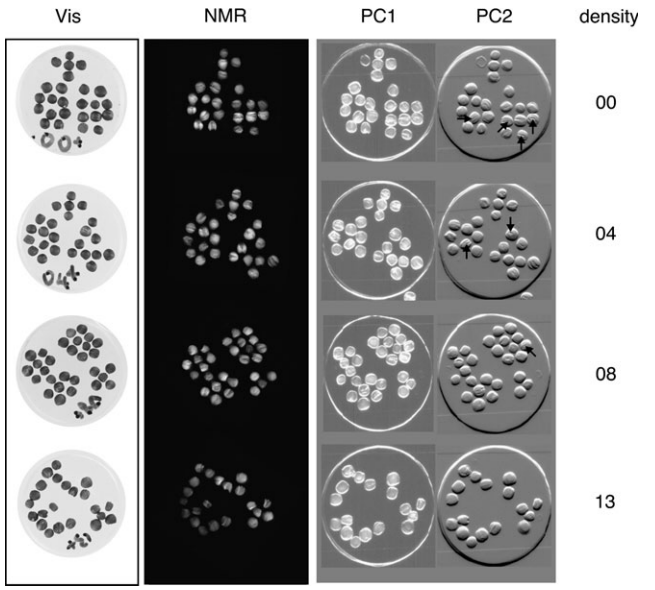

Fig. 2. Visible, NMR, and DEI images of density-sorted canola seeds. Seeds were sorted in low-polarity solutions of different densities, washed, and glued onto Lucite discs. Each disc was photographed and imaged using NMR and DEI. The NMR imaging used a 5 mm slice and the DEI data were processed using PCA. Density groups were, from top to bottom, $d < 1.00$, $d < 1.04$, $d < 1.08$, $d < 1.13$. Features observed include hypocotyl–root axes, seed coats, cotyledon outlines, and air cavities (arrows). Pixel size was approximately 21 μm and 50 μm for NMR and DEI, respectively. Canola seeds were approximately 2 mm in diameter.

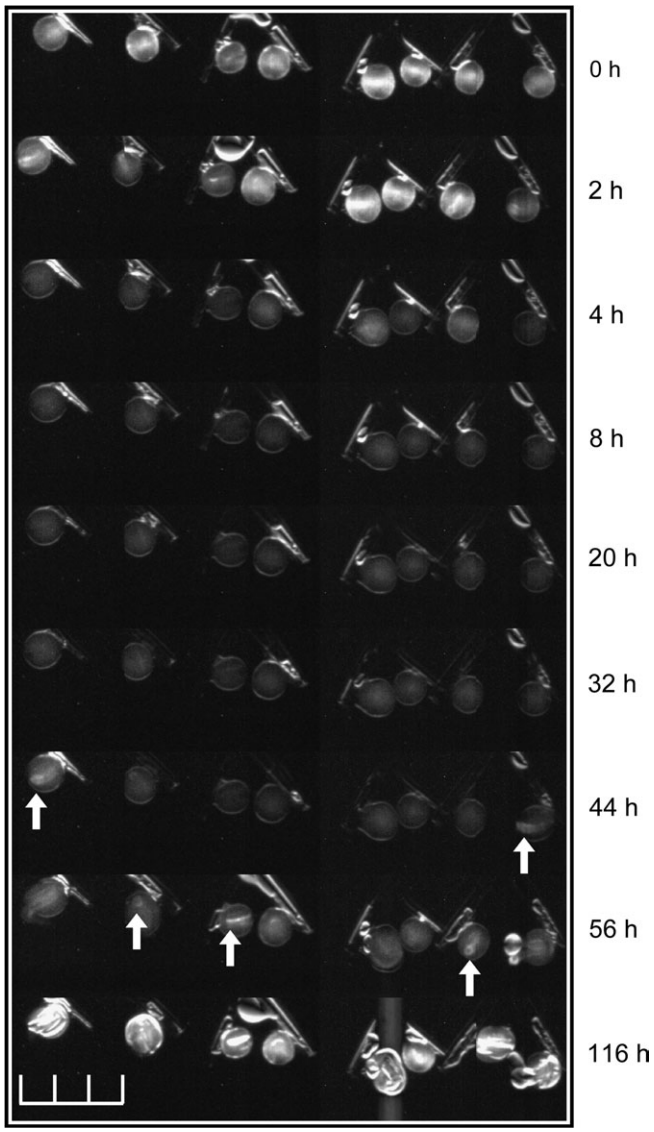

Fig. 3. DEI of germinating canola seeds. Canola seeds attached to pipette tips were imaged using DEI over a time course (0, 2, 4, 8, 20, 32, 44, 56, and 116 h after imbibition). Hypocotyl–root axes (arrows) and seed coats can be seen in this image. The standard deviation over the rocking curve for each pixel was calculated and used as the basis for pixel intensity. The grey-scale intensity was modified to deliver the maximum contrast. Gaps between these eight representative seeds were removed. Scale bar = 6 mm with 2 mm graduations.

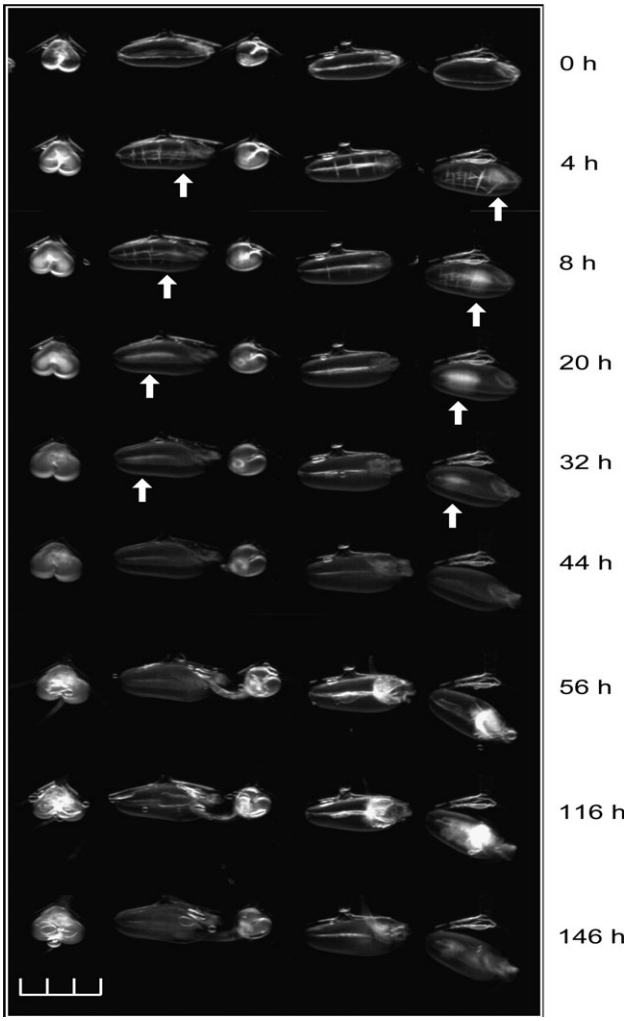

Fig. 4. DEI of germinating wheat. Wheat caryopses were attached to pipette tips and imaged using DEI at 0, 4, 8, 20, 32, 44, 56, 116, and 146 h after imbibition. The embryo axis, scutellum, pericarp furrow, cracks in the pericarp, and the wave of starch gelatinization or hydration (arrows) were observed. These features overlap in the seeds oriented in cross-section and were more difficult to discern. At later time points, coleoptiles and roots can also be observed. A single group of five caryopses is displayed. Scale bar = 6 mm with 2 mm graduations.

The location and orientation of canola hypocotyl–root axes could be identified, especially in the 2 h post-imbibition image (Fig. 3). Refraction decreased in the 4, 8, 16, and 20 h images, with seed coats causing most of the observed X-ray refraction. The reduced X-ray refraction by the radicle indicates that the density difference between the hypocotyl–root axis and cotyledons was minimal during this period.

A change in density or ordering of the tissues was observed in the radicles just prior to emergence. This was first noticeable in two seeds in the 44 h image, and in the 56 h image for the remaining seeds (Fig. 3, arrows). Emerged radicles were observed in the 56 h and 116 h images; however, air bubbles attached to the organ and trapped within the seed coat obscured some of the images.

A number of interesting anatomical structures were observed in germinating wheat caryopses (Fig. 4). The embryo, scutellum, and pericarp furrow were observed at 0 h imbibition. The embryo axis and the furrow were most visible from 8 to 44 h and 0 to 20 h after imbibition, respectively, in both longitudinal and cross-section. The nucellar projection and endosperm cavity, above the pericarp furrow, were also discernible. The intensity of these regions decreased over time, however. This may be due to absorption of water by hydrophilic compounds present (Bradbury *et al*., 1956) or by swelling of the tissues surrounding this region, which would reduce the size of any air cavities present. Either phenomenon would reduce the density-dependent X-ray refraction. In the later images, roots and coleoptiles were observed emerging from caryopses in both orientations.

A region of altered density was observed to migrate from the scutellum to the adaxial end of longitudinally oriented seeds (Fig. 4, arrows). The density difference was first apparent 4 h after imbibition and was still observable in the 32 h image. The change in endosperm density was also observed in cross-section. From the cross-section images it is apparent that the change in density is limited to the endosperm and does not overlap the pericarp. The changes in density may be due to either hydration or catabolism of storage molecules in the endosperm, i.e. changes to starch grains or protein body structure.

Cracks in the pericarp were observed in the longitudinally aligned seeds starting 2 h after imbibition. The size and number of cracks decreased over time and disappeared 20 h after imbibition. These cracks were obscured in cross-section by the changes in endosperm density.

Supplementary Fig. S6 (available at *JXB* online) is provided as an example of the fine detail it is possible to achieve with DEI when a high-resolution detector is used. The detector element size was 10 μm×10 μm for this image.

Discussion

This paper focused on using DEI to observe seed anatomy and germination. Features that were observed using DEI included the hypocotyl–root axis, seed coat/pericarp, pericarp cracks, cotyledons, scutellum, wheat embryo axis, roots, and coleoptiles. Air cavities associated with the hypocotyl–root axis in some canola seeds and changes in starch structure were also observed. Although this paper has focused on seeds, the images presented here and the demonstrations of how this technique can be used in medical imaging make it clear that, in the future, DEI will be a useful tool for examining plant anatomy and physiology.

The novel basis of contrast, non-destructiveness, easy sample preparation, and depth of observation make DEI

complementary to other imaging techniques such as conventional X-ray radiography, confocal microscopy, and NMR. Some of this complementarity arises as each technique examines a different physical or chemical property. Conventional X-ray imaging has been used to reveal insect infestation (Schatzki and Fine, 1988; Karunakaran *et al*., 2003; Haff and Slaughter, 2004) and seed damage (Milner *et al*., 1952*a*; de Carvalho *et al*., 1999; Létang *et al*., 2002), and to indicate seed quality (Simak and Sahlén, 1981; Foucat *et al*., 1993; Downie *et al*., 1999); however, signal:noise ratios (e.g. Pechen and Keller, 1988), edge definition, and the potential for radiation damage are more problematic than with DEI. NMR imaging is excellent for observing the distribution of oil or water in a sample (e.g. Song *et al*., 1998; Pietrzak *et al*., 2002; Manz *et al*., 2005), while confocal microscopy is good for imaging the location of molecules at a subcellular level in living cells, down to ~100 μm tissue depths (Haseloff, 2003). Spatial resolution of both NMR and X-ray imaging is partially determined by the capability of the detector. Digital detectors with a 10 μm pixel size are available for X-ray imaging (for example, see Supplementary Fig. S6 available at *JXB* online) while film may show much more detail, but is much more laborious to use. Pixel size for NMR detectors may be as small as 5 μm and is also dependent on the number of scans made. The images in this paper were captured using a detector with 50 μm×50 μm pixels.

DEI observations are also complementary to X-ray PCI (Hwu *et al*., 2004; Cloetens *et al*., 2006) and OPT (Lee *et al*., 2006). PCI and DEI both use refraction to provide contrast. The difference is that DEI/MIR quantifies photons refracted and scattered at a number of different angles, whereas it is difficult to separate this information from PCI data. Thus, using DEI, information about sample density can be obtained. However, data collection is much slower and potentially causes greater radiation damage when using DEI compared with PCI. Both DEI and PCI may be used to generate three-dimensional tomographic images of samples (Cloetens *et al*., 2006; T Kao, C-J Liu, X Yu, *et al*., unpublished results). OPT provides high-resolution three-dimensional images of plant tissues and may be used to examine gene expression (Lee *et al*., 2006). One disadvantage is that observation of embedded or opaque structures requires tissue clearing (resulting in cell death) and so developmental changes in single individuals cannot be examined. As has been demonstrated, it is possible to follow development in single individuals using DEI over a number of time points.

The non-destructive nature of DEI allows different physical or chemical attributes of the samples to be examined using other imaging techniques. The non-destructive nature of DEI is also an advantage in developmental studies as changes in a single individual can be examined over several time points. Some possible future investigations demonstrating the complementarity of DEI with other imaging techniques include examining water uptake in imbibing seeds, following embryo/seed/silique development or abortion, tracing development in plants with anatomical mutations, examining apical meristem development, imaging roots growing in an opaque matrix, and observing seed herbivory or endoparasitism.

DEI provided clearer, less noisy images than those obtained using conventional X-ray imaging (compare Milner *et al*., 1952*a*, *b*; Pechen and Keller, 1988; Foucat *et al*., 1993; Haff and Slaughter, 2004). DEI images are sharper than conventional X-ray images because higher energy X-rays (40–60 keV compared with 6–20 keV) are used and refracted X-rays are measured as data. X-rays refract at density interfaces, regardless of the energy of the incident photons, and so tissue boundaries are observable using DEI as tissues and organs have different densities. An additional advantage of using high-energy X-rays is that the absorbed radiation dose is low. The amount of radiation absorption has been calculated to be <1% of that delivered by a mammogram (approximately 0.12 mGy per exposure; Li *et al*., 2003) and was not expected to affect germination or growth significantly. In this experiment, canola and wheat germination did not appear to be affected by nine or ten exposures, although mutagenic effects of the X-rays were not analysed.

In canola seeds, the outline of the hypocotyl–root axis in longitudinal section was observed as this organ has a different density from the surrounding cotyledons (compare the NMR images in Fig. 2, where the low oil-content/high-density hypocotyl–root axes contrast the higher oil content/lower density cotyledons). In longitudinal section, minimal X-ray refraction was observed in the centre of the hypocotyl–root axis. By contrast, hypocotyls observed in cross-section caused a large amount of X-ray refraction, although primarily from the region occupied by the ground meristem. This may be due to the columnar arrangement of ground meristem cells along the axis of the beam, aligning cell walls and their cellulose fibrils, which would cause a large amount of photon scatter. Further supporting this hypothesis is the observation that the more-ordered ground meristem refracted X-rays to a greater extent than the less-ordered procambium, These data suggest that detailed analysis of both tissue anatomy and composition may be carried out using DEI or MIR. The use of MIR is appropriate as three components, attenuation, refraction, and scatter, are extracted from the data (Wernick *et al*., 2003). Quantification of refraction and scatter gives an indication of density and molecular order, respectively.

MIR deconvolution could be used to separate the refraction and scattering components of the data for hypocotyls in cross-section. A high scatter to refraction

ratio would indicate that structured order within the radicles was responsible for their intense signal. Another tissue that was clearly visible using DEI was the seed coat. The canola seed coat is more dense than other parts of the seed (Thakor *et al.*, 1995) and thus caused significant X-ray refraction. Further analysis of the data could provide useful information about the amount of refraction and scatter resulting at each pixel, which could then be interpreted as relative density and concentration of ordered molecules, respectively. This information could be of use for studying tissue composition. For example, in the case of developing seeds, patterns of seed storage molecule accumulation could be followed as the major components (starch, protein, and oil) have significantly different densities and atomic arrangements.

The clearest images, i.e. those with the greatest contrast and least noise, were obtained with the standard deviation images and the first two or three components of the PCA. The first two or three principle components could be classified into two types of images: those that resembled the attenuation and/or refraction images and those that showed regions with the greatest difference in density. One disadvantage of the standard deviation and PCA images is that quantitative information about the extent of X-ray refraction occurring was lost, i.e. assignment of each principle component to a type of X-ray interaction (attenuation, refraction, and scatter) is lost and requires observer interpretation. Information about the degree of refraction may still be extracted from the raw data (see Fig. 1), or derived using the MIR technique.

The use in the present study of PCA on the data was only possible because the samples were relatively flat. Thicker samples, with overlapping layers of tissue acting to produce multiple overlying sources of scatter, would interfere with the analysis. For thicker samples, MIR may be used to elucidate the attenuation, refraction, and scatter components (Wernick *et al.*, 2003; Muehleman *et al.*, 2006). The present use of the first three PCA components in false colour images assumed that the overlying regions of scatter were minimal (see supplementary figures available at *JXB* online). Future work is necessary to compare the images of seeds obtained using MIR and PCA treatment of the data.

The principles behind DEI and NMR imaging are different; however, the same gross anatomical structures could be observed using both techniques, the most obvious being hypocotyl–root axes. The NMR images could have been more detailed if a finer slice had been used. Using a 0.3 mm slice, it was possible to discern the outline of the inner and outer cotyledons (not shown). These organs were also visible in some of the canola seeds using DEI, depending on orientation. Using a false colour representation of the first three components from the PCA increased the contrast substantially, allowing observation of both cotyledons in all seeds with suitable orientations (see Supplementary Fig. S2 available at *JXB* online).

Some features are more visible using one technique than the other. Seed coats and air cavities were easily resolved using DEI. Conversely, relative oil concentrations are more difficult to observe using DEI compared with NMR. All these data could be obtained using both techniques if the experimental set-up was altered. For example, infusion of a contrasting agent into the seeds would allow air spaces to be observed using NMR, and further studies of the refractive and scattering properties of oleosomes (or starch granules) could be performed to model different concentrations of these structures. See Table 2 for a summary comparing DEI and NMR.

Perhaps the most interesting DEI observations were of germination. The region of altered density that moved from the scutellum to the apex in germinating wheat caryopses was visible to some degree in all the caryopses studied and was striking in the right-most individual (Fig. 4 and Supplementary Fig. S5 available at *JXB* online). The density changes may have been due to Phase I or Phase II of imbibition (Bewley, 1997; Krishnan *et al.*, 2003; Manz *et al.*, 2005) or a wave of storage molecule

Table 2. *DEI and NMR comparison*

	NMR imaging	DEI
Basis of contrast	Differing concentrations of atoms containing odd numbers of electrons	Different densities (at tissue boundaries) Presence of ordered structures (cells aligned in columns parallel to beam, structured molecules such as starch or protein bodies)
Sample set-up	Placement in NMR tube	Immersion in liquid
Detector resolution (current)	5 μm	10 μm
Non-destructive?	Yes	Yes (minimal absorbed radiation damage)
Further refinements	Spectroscopy to distinguish components Infusion with contrast agents	Computed tomography MIR to separate attenuation, refraction, and scatter components
Limitations	Size of samples in laboratory-based machines Typically used for oil or water location	Transmission view: structures in thicker tissues will overlap Only possible using a synchrotron at present

hydrolysis (starch or protein). The timing of the event, starting at 2 h and proceeding until 32 h after imbibition, excludes the possibility that Phase I of imbibition (Bewley, 1997) is being observed, as this stage occurs between 0 h and 6 h; however, this does not exclude the possibility of the event being due to free water spreading throughout the kernel, as occurs in Phase II of imbibition (Krishnan *et al*., 2003). Further evidence that the event being observed is related to water uptake is the similarity of the DEI images to NMR images of imbibing oat caryopses (Hou *et al*., 1997).

The change in density observed during germination may be a direct observation of storage molecule catabolism. The timing of the event matches observations of gibberellin secretion and increased hydrolase activity occurring during germination (especially bound β-amylase release from starch granules; Fincher, 1989), the area of density difference is limited to the endosperm and does not overlap the aleurone or pericarp, and the X-ray refractive index of starch changes during gelatinization (Lemke *et al*., 2004). The event could possibly be due to the enzymatic hydrolysis of storage proteins; however, this is unlikely to be the cause as the extent of protein breakdown is minimal after 1 d (Preston and Kruger, 1979; Bigiarini *et al*., 1995) and the small change in protein degradation would be difficult to observe. Higher resolution images of germinating seeds, possibly in conjunction with NMR imaging (for examples, see Foucat *et al*., 1993; Krishnan *et al*., 2003; Manz *et al*., 2005), would help confirm that a physiological event was observed using DEI. Such an experiment would also demonstrate the complementarity of DEI and NMR imaging and may provide novel information about processes occurring during germination and emergence.

Another developmental change observed in germinating wheat was the appearance and subsequent disappearance of cracks in the pericarp. Cracks in cereal caryopses have been observed using conventional X-ray imaging (Milner *et al*., 1952*b*; de Carvalho *et al*., 1999); however, tracing the disappearance of these cracks has not been reported. The cracks observed using DEI appear to be limited to the pericarp, unlike those observed in maize which were present in the endosperm and sometimes the embryo axis (de Carvalho *et al*., 1999), and thus this observation may be a new phenomenon, different from the cracks resulting from mechanical damage during harvesting. As postulated earlier, if water uptake is observable using DEI, the observed pericarp cracks are unlikely to be the result of mechanical damage as water permeated through these sites in scarified oat caryopses (Hou *et al*., 1997). These observations, along with the change in the refractive properties of the pericarp furrow, nucellar projection, and endosperm cavity suggest that DEI can be used to observe water uptake by seeds.

The changes to the canola seed images up until the 20 h image may also be related to water uptake. At first the hypocotyl–radicle axis is visible; however, during imbibition, the density changes such that it becomes similar to the adjacent cotyledons. It is possible that the hypocotyl–radical axis takes up water at a rate different from the cotyledons, which is observed as a change in organ density using DEI. Alternatively, hypocotyl–radicle density may change during imbibition as cells expand and air cavities in the organ are lost (Cloetens *et al*., 2006).

The data obtained in the germination images will complement observations on water uptake obtained by NMR (Foucat *et al*., 1993; Song *et al*., 1998; Pietrzak *et al*., 2002; Manz *et al*., 2005). Other physiological changes were observed in canola radicles during imbibition and just prior to emergence that may have been related to altered water content. The change in radicle density may be due to the increase in turgor pressure that is suspected to allow the organ to penetrate the surrounding tissues (Bewley, 1997). These data suggest that DEI may be an alternative way of observing turgor pressure in living organs.

Some of the disadvantages associated with DEI are the necessity for a bright, coherent X-ray source, distinguishing features overlying one another, the potential for radiation damage to the sample, and the need to immerse the sample. Currently, DEI requires a bright, coherent X-ray source, essentially a synchrotron. Although access to many of these facilities is free to academic researchers (based on scientific merit), the small number of beamlines currently performing DEI may limit its widespread use. This situation will improve in the future as several DEI-capable beamlines are planned or under construction worldwide. Furthermore, work is underway to develop a laboratory-based device capable of performing DEI.

One difficulty with interpreting DEI images is that overlying structures may obscure one another. This problem may be alleviated somewhat by using false-colour representations of the attenuation, refraction, and scatter data. Distinguishing overlapping features becomes simpler as each tissue has a different absorption coefficient, density, and ordered macromolecule composition, i.e. each tissue will have a different colour in the image (Wernick *et al*., 2003; Muehleman *et al*., 2006). Another way of distinguishing overlapping tissues is to perform computed tomography. Tomography presents the data in three dimensions, and slices through the sample may be observed.

The problem with tomography is that a large number of images must be captured, resulting in greater radiation exposure. Radiation exposure with two-dimensional DEI is low; however, for some variations of the technique, such as MIR and tomography, or during developmental studies, multiple exposures are necessary. The effects of radiation damage can be reduced by reducing exposure times and frequencies or by reducing the number of data points included in the rocking curve. Another way of

reducing radiation damage could be to increase the energy of the X-rays to 60 keV or to use PCI if rocking curve data are not required.

Finally, one of the difficulties associated with DEI is that the samples are often immersed in liquid to reduce the density difference at the surface of the object and its surrounds. Imaging in air is possible; however, the large density difference at the air–sample interface results in a large amount of refraction. One solution to this problem is to immerse the samples in media with different biological, chemical, and physical properties, such as ethanol or glycerine.

DEI could potentially complement observations of living plant tissues made using confocal microscopy or NMR. The ability to image anatomical structures and physiological events non-destructively will be useful for researchers studying plant development. Advantages to using DEI include the ability to observe tissues embedded within other tissues, the use of density and ordered structures within a sample as contrast agents, and simple sample preparation. Future developments of DEI, MIR, and other X-ray refraction-based techniques such as phase contrast may include computed tomography for three-dimensional imaging, the use of high-resolution detectors to visualize cellular structures (Colbert *et al*., 2001; Hwu *et al*., 2004), and elemental analysis via X-ray fluorescence analysis (a basic demonstration of this will be presented in another paper by L Young, N Westcott, C Christensen *et al*.).

Supplementary data

Fig. S1. Schematic of canola seed observed in cross- (top) and longitudinal (bottom) section through the hypocotyl–root axis.

Fig. S2. High resolution image of canola seed DEI analysed using PCA components 1–3 (top three images). The first three components were assigned to the red, blue, green and blue, red, green channels, respectively, for the two coloured images.

Fig. S3. High resolution visible, NMR, and DEI images showing all seed discs. The density of seeds on each disc is indicated on the side (e.g. 00 = $d < 1.00$). + indicates populations enriched for seeds containing air cavities, − indicates populations with a reduced number of seeds with air cavities.

Fig. S4. High resolution images of germinating canola seeds, from top to bottom, 0, 2, 4, 8, 20, 32, 44, 56, 116 h after imbibition. From left to right, principle components 1–3 and a colour composite based on these three images using the hue, intensity, and saturation system.

Fig. S5. High resolution images of germinating wheat caryopses. As per Supplementary Fig. S4 without the 2 h after-imbibition image but including the 156 h image. Two false colour images are shown, with different combinations of attenuation, refraction, and scatter images assigned to the red, green, and blue channels.

Fig. S6. Image of disc 08 (Fig 2) using an X-ray detector with 10 μm×10 μm pixel sizes. Several seeds have fallen off but the cyanoacrylate adhesive still remains. This image shows the summed images from across the rocking curve.

Acknowledgements

The authors are grateful to the following sources for providing funding: Saskatchewan Synchrotron Institute, the 'Enhancing Canola through Genomics' project from Genome Prairie, US Department of Energy contract no. DE-AC02-98CH10886 and by NIH grant R01 AR48292.

References

Bewley JD. 1997. Seed germination and dormancy. *The Plant Cell* **9,** 1055–1066.

Bigiarini L, Pieri N, Grilli I, Galleschi L, Capocchi A, Fontanini D. 1995. Hydrolysis of gliadin during germination of wheat seeds. *Journal of Plant Physiology* **147,** 161–167.

Bouwstra JA, Gooris GS, Bras W, Talsma H. 1993. Small angle X-ray scattering: possibilities and limitations in characterization of vesicles. *Chemistry and Physics of Lipids* **64,** 83–98.

Bradbury D, MacMasters MM, Cull IM. 1956. Structure of the mature wheat kernel. II. Microscopic structure of pericarp, seed coat, and other coverings of the endosperm and germ of Hard Red Winter Wheat. *Cereal Chemistry* **33,** 342–360.

Chapman D, Thomlinson W, Johnston RE, Washburn D, Pisano E, Gmur N, Zhong Z, Menk R, Arfelli F, Sayers D. 1997. Diffraction enhanced x-ray imaging. *Physics in Medicine and Biology* **42,** 2015.

Cloetens P, Mache R, Schlenker M, Lerbs-Mache S. 2006. Quantitative phase tomography of *Arabidopsis seeds* reveals intercellular void network. *Proceedings of the National Academy of Sciences, USA* **103,** 14626–14630.

Colbert T, Till BJ, Tompa R, Reynolds S, Steine MN, Yeung AT, McCallum CM, Comai L, Henikoff S. 2001. High-throughput screening for induced point mutations. *Plant Physiology* **126,** 480–484.

de Carvalho MLM, van Aelst AC, van Eck JW, Hoekstra FA. 1999. Pre-harvest stress cracks in maize (*Zea mays* L.) kernels as characterized by visual, X-ray and low temperature scanning electron microscopial analysis: effect on kernel quality. *Seed Science Research* **9,** 227–236.

Donald AM, Kato KL, Perry PA, Waigh TA. 2001. Scattering studies of the internal structure of starch granules. *Starch – Stärke* **53,** 504–512.

Downie B, Gurusinghe S, Bradford KJ. 1999. Internal anatomy of individual tomato seeds: relationship to abscisic acid and germination physiology. *Seed Science Research* **9,** 117–128.

Fincher GB. 1989. Molecular and cellular biology associated with endosperm mobilization in germinating cereal grains. *Annual Review of Plant Physiology and Plant Molecular Biology* **40,** 305–346.

Foucat L, Chavagnat A, Renou J-P. 1993. Nuclear magnetic resonance micro-imaging and X-radiography as possible techniques to study seed germination. *Scientia Agricola* **55,** 323–331.

Haff RP, Slaughter DC. 2004. Real-time X-ray inspection of wheat for infestation by the granary weevil. *Sitophilus granarius (L.). Transactions of the ASAE* **47,** 531–537.

Haseloff J. 2003. Old botanical techniques for new microscopes. *BioTechniques* **34,** 1174–1182.

Hou JQ, Kendall EK, Simpson GM. 1997. Water uptake and distribution in non-dormant and dormant wild oat (*Avena fatua* L.) caryopses. *Journal of Experimental Biology* **48,** 683–692.

Hwu Y, Tsai WL, Chang HM, *et al*. 2004. Imaging cells and tissues with refractive index radiology. *Biophysical Journal* **87,** 4180–4187.

Jenkins PJ, Cameron RE, Donald AM. 1993. A universal feature in the structure of starch granules from different botanical sources. *Starch – Stärke* **45,** 417–420.

Jenner CF, Xia Y, Eccles CD, Callaghan PT. 1988. Circulation of water within wheat grain revealed by nuclear magnetic resonance micro-imaging. *Nature* **336,** 399–402.

Karunakaran C, Jayas DS, White NDG. 2003. X-ray image analysis to detect infestations caused by insects in grain. *Cereal Chemistry* **80,** 553–557.

Krishnan P, Joshi DK, Nagarajan S, Moharir AV. 2003. Characterisation of germinating and non-germinating wheat seeds by nuclear magnetic resonance (NMR) spectroscopy. *European Biophysics Journal* **33,** 76–82.

Lee K, Avondo J, Morrison H, Blot L, Stark M, Sharpe J, Bangham A, Coen E. 2006. Visualizing plant development and gene expression in three dimensions using optical projection tomography. *The Plant Cell* **18,** 2145–2156.

Lemke H, Burghammer M, Flot D, Rössle M, Riekel C. 2004. Structural processes during starch granule hydration by synchrotron radiation microdiffraction. *Biomacromolecules* **5,** 1316–1324.

Létang J-M, Peix G, Droulez L. 2002. Automatic selection of seeds using pattern recognition techniques in high resolution x-ray images. *NDT.net* **7,** http://www.ndt.net/article/ecndt02/412/412.htm.

Li J, Zhong Z, Lidtke R, Kuettner KE, Peterfy C, Aliyeva E, Muehleman C. 2003. Radiography of soft tissue of the foot and ankle with diffraction enhanced imaging. *Journal of Anatomy* **202,** 463–470.

Manz B, Müller K, Kucera B, Volke F, Leubner-Metzger G. 2005. Water uptake and distribution in germinating tobacco seeds investigated *in vivo* by nuclear magnetic resonance imaging. *Plant Physiology* **138,** 1538–1551.

Milner M, Lee MR, Katz R. 1952*a*. Radiography applied to grain and seeds. *Food Technology* **6,** 44–45.

Milner M, Shellenberger JA, Lee MR, Katz R. 1952*b*. Internal fissuring of wheat due to weathering. *Nature* **170,** 533.

Mollenhauer J, Aurich ME, Zhong Z, Muehleman C, Cole AA, Hasnah M, Oltulu O, Kuettner KE, Margulis A, Chapman LD. 2002. Diffraction-enhanced X-ray imaging of articular cartilage. *Osteoarthritis and Cartilage* **10,** 163–171.

Muehleman C, Li J, Zhong Z, Brankov JG, Wernick MN. 2006. Multiple-image radiography for human soft tissue. *Journal of Anatomy* **208,** 115–124.

Paris O, Zizak I, Lichtenegger H, Roschger P, Klaushofer K, Fratzl P. 2000. Analysis of the hierarchical structure of biological tissues by scanning X-ray scattering using a micro-beam. *Molecular Biology of the Cell* **46,** 993–1004.

Pechen PM, Keller WA. 1988. Identification of potentially embryogenic microspores in *Brassica napus*. *Physiologia Plantarum* **74,** 377–384.

Pietrzak LN, Fregeau-Reid J, Chatson B, Blackwell B. 2002. Observations on water distribution in soybean seed during hydration processes using nuclear magnetic resonance imaging. *Canadian Journal of Plant Science* **82,** 513–519.

Preston KR, Kruger JE. 1979. Physiological control of exo- and endoproteolytic activities in germinating wheat and their relationship to storage protein hydrolysis. *Plant Physiology* **64,** 450–454.

Schatzki TT, Fine TA. 1988. Analysis of radiograms of wheat kernels for quality control. *Cereal Chemistry* **65,** 233–239.

Simak K, Sahlén K. 1981. Comparison between the x-radiography and cutting tests used in seed quality analysis. *Seed Science and Technology* **9,** 205–227.

Song HP, Delwiche SR, Line MJ. 1998. Moisture distribution in a mature soft wheat grain by three-dimensional magnetic resonance imaging. *Journal of Cereal Science* **27,** 191–197.

Thakor NJ, Sokhansanj S, McGregor I, McCurdy S. 1995. Dehulling of canola by hydrothermal treatments. *Journal of the American Oilchemists' Society* **72,** 597–602.

Wernick MN, Wirjadi O, Chapman D, Zhong Z, Galatsanos NP, Yang Y, Brankov JG, Oltulu O, Anastasio MA, Muehleman C. 2003. Multiple-image radiography. *Physics in Medicine and Biology* **48,** 3875–3895.

Young L, Jalink H, Denkert R, Reaney M. 2006. Factors affecting the density of *Brassica napus* seeds. *Seed Science and Technology* **34,** 633–645.